Int. J. Multiphase Flow Vol. 9, No. 4, pp. 349–366, 1983
Printed in Great Britain.

0301-9322/83 $3.00 + .00
Pergamon/Elsevier

AIR–WATER COUNTERCURRENT ANNULAR FLOW

D. BHARATHAN
Solar Energy Research Institute, Golden, CO 80401, U.S.A.

and

G. B. WALLIS
Thayer School of Engineering, Dartmouth College, Hanover, NH 03755, U.S.A.

(*Received* 5 *April* 1982; *in revised form* 10 *October* 1982)

Abstract—Experimental results on investigation of countercurrent air–water flows in vertical circular tubes of a range of diameters are reported. Based on the influence of tube end geometries on measured countercurrent fluxes, liquid fraction, and pressure gradients, analogies between countercurrent gas–liquid flow and other more familiar flows in internal geometries are indicated. Interfacial momentum transfer between the phases is characterised by empirical friction factors. The dependence of interfacial friction factors on tube diameter is used to suggest a basis for generalizing the results using a dimensionless correlation involving surface tension.

INTRODUCTION

Countercurrent flow of a gas and a liquid occurs in industrial gas–liquid contact devices such as wetted- or packed-column towers. Under these conditions an annular flow pattern in which a continuous liquid film flows along the wall and the gas flows in a central "core" is prevalent. Accompanying this, for a given flow channel geometry, there occurs a flow limiting process termed "flooding", when for a given flux, the liquid flow attains a practical maximum and cannot be further increased without decreasing the gas flux. Flooding is one of the many processes likely to occur in postulated loss-of-coolant accidents in water-cooled nuclear reactors. The phenomenon may limit the penetration of emergency coolant into the core region from above (Lahey 1977).

Under flooding conditions the peculiar nature of pressure drop vs flow characteristics leads to many instabilities and non-uniform flow patterns in parallel channels (Bharathan 1978b).

Early investigations of flooding in circular tubes were carried out, among others, by Wallis (1969) and Hewitt *et al.* (1963). Wallis (1969) proposed a simple correlation to relate the limiting fluxes. He also put forth the ideas that maximum limiting fluxes lie on an envelope of a set of constant liquid-fraction curves and that end conditions cause the measured fluxes to be smaller and fall within the envelope (Wallis 1970). Imura *et al.* (1977) summarize and review the various proposed correlations to relate flooding velocities to liquid flow rates and fluid properties. Analytical studies to predict the onset of flooding based on interfacial instability were proposed by Shearer (1965), Cetinbudakler (1969), and by Imura (1977). A comprehensive survey of the various works on vertical two-phase countercurrent flooding can be found in Tien & Lin (1979).

Empirical approaches to flooding and associated transfer process involve defining suitable transfer coefficients. In the case of air and water, where momentum transfer is the dominant process, the interfacial shear stresses are usually described by interfacial friction factors. Attempts to relate the friction factor to the liquid film thickness can be found in many instances. Hewitt & Hall-Taylor (1970) review the historical development of correlations relating friction factor to the film thickness indirectly through an "equivalent surface roughness".

The primary objectives of the present study are to identify the nature of countercurrent flow hydraulics, the mechanism limiting the countercurrent fluxes, and the scaling laws

governing the phenomena. Experimental results from investigations of air and water flow in long vertical Lucite tubes of diameters ranging from 6.4 to 152 mm are reported. The set of steady-state measurements includes limiting fluxes, pressure losses, pressure gradients, and in certain instances, liquid fraction. The influences of tube end geometries on the limiting gas and liquid fluxes are identified. Important flow regimes in which either the wall shear or the interfacial shear is dominant are isolated. The interfacial shear is quantitatively described by an empirical interfacial friction factor which is a function of the liquid film thickness, the tube diameter, interfacial surface tension, and gravity. With the addition of a suitable wall friction factor a theory to represent countercurrent annular gas–liquid flow is developed. The theory is shown to yield multiple solutions for liquid fraction and pressure gradient consistent with experimental observations. Comparisons of measured flow characteristics with the theory are presented. The present approach also yields a method for extending the test results from small tubes to large tubes and annular flow passages.

ANALYTICAL BACKGROUND

In a vertical countercurrent annular flow the liquid film is neither stationary nor uniform within the tube. However, for a given section of a long tube, an average film thickness δ may be assigned to the liquid film as shown in figure 1. Gas, which may contain suspended liquid droplets, flows upward through the central core, while the liquid drains downward in an agitated annular film. The gas–liquid interface generally appears wavy. Neglecting the volume of entrained droplets, the void fraction, α, or the fractional volume occupied by the gas in a given section of the channel is

$$\alpha = \left(1 - \frac{2\delta}{D}\right)^2. \qquad [1]$$

Here D is the inner diameter of the tube.

Ignoring compressibility effects and variations of liquid film thickness, for steady flows a force balance on the gas "core" yields:

$$\frac{dp}{dz} + \rho_G g + \frac{4\tau_i}{D\sqrt{\alpha}} = 0. \qquad [2]$$

Here p is the static pressure; z the vertical coordinate; ρ_G the gas density; g the acceleration due to gravity; and τ_i is the interfacial shear stress which may consist mostly of form drag over protruding liquid waves.

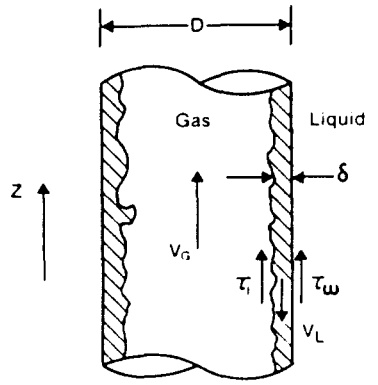

Figure 1. Sketch of annular countercurrent gas–liquid flow in vertical tube.

Since the nominal gas velocity v_G is often much greater than that of the liquid v_L, the interface may be assumed stationary and thus, analogous to single-phase flows, an interfacial friction factor f_i can be defined as

$$f_i = \frac{2\tau_i \alpha^2}{\rho_G j_G^2} \quad [3]$$

where j_G is the mean volumetric gas flux.

For most practical cases, $(dp/dz) \gg \rho_G g$, and thus

$$f_i = \frac{-(dp/dz)D\alpha^{5/2}}{2\rho_G j_G^2}$$

or

$$f_i = \frac{-(dp/dz)^* \alpha^{5/2}}{2j_G^{*2}} \quad [4]$$

where the non-dimensional pressure gradient and gas flux are given by respectively,

$$(dp/dz)^* = \frac{(dp/dz)}{(\rho_L - \rho_G)g} \quad [5]$$

and

$$j_G^{*2} = \frac{\rho_G j_G^2}{(\rho_L - \rho_G)gD}. \quad [6]$$

Here ρ_L is the liquid density.

By considering the force balance for the entire cross section of the tube, one may deduce that

$$(dp/dz) + \rho_G g + (1-\alpha)(\rho_L - \rho_G)g = \frac{4\tau_w}{D} \quad [7]$$

where τ_w is the shear stress opposing the downward liquid flow. Here again, a wall friction factor f_w may be defined as

$$f_w = \frac{2\tau_w(1-\alpha)^2}{\rho_L j_L^2} \quad [8]$$

where j_L is the mean volumetric downward liquid flux.

When there is no net downward liquid flow, but there exists a liquid film within a tube, f_w can not be adequately defined. However, under this circumstance, the pressure-gradient measurements indicate that the wall shear stress becomes insignificant in relation to the interfacial shear stress and the magnitude of f_w by itself is of no practical significance.

For air–water countercurrent flows, for pipe diameters in the range 1–10 cm, many measured air and water flow rates under flooding conditions are known to correlate well by the relation proposed by Wallis (1969),

$$j_G^{*1/2} + m j_L^{*1/2} = C \quad [9]$$

where

$$j_L^{*2} = \frac{\rho_L j_L^2}{(\rho_L - \rho_G) g D} \qquad [10]$$

and m and C are non-dimensional constants which depend upon liquid inlet and exit geometry. For turbulent air–water flows, the constant m attains a value close to unity (Wallis 1969).

In [9], the parameters j_G^* and j_L^* represent the balance between inertial and gravity forces. In addition to these, other forces which merit considerations are the viscous forces in the gas and liquid phases and the interfacial surface tension. The relative importance of the various forces in general varies with the physical flow patterns, which are discussed in the following sections.

REGIMES IN FLOODING

When an annular liquid film is present within the tube, countercurrent flow characteristics may be divided into three regimes depending upon the relative magnitudes of interfacial and wall shear stresses. These regimes, as indicated in a typical plot of $(1-\alpha)$ vs j_G^* in figure 2, are:

(A) A region where the interfacial shear stress τ_i is negligible compared to the wall shear stress impeding the liquid flow. Under this condition, the liquid that enters the tube at the top end flows downward undisturbed by the gas flow over the entire tube length and the bottom end. However, at any gas flux, the downward liquid flux is limited by a relation such as [9]. Thus, the restrictions to liquid flux through the tube occurs at the tube's top end. This region is labelled "smooth film" in figure 2.

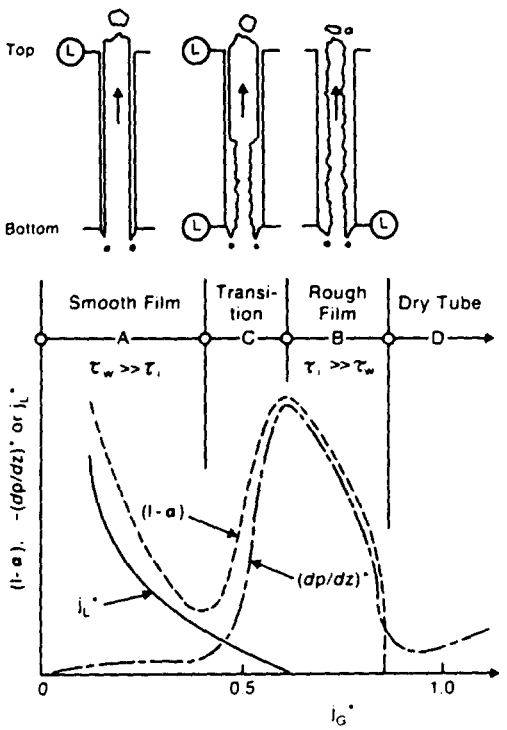

Figure 2. Typical qualitative variations of measured liquid flux, liquid fraction and pressure gradient with gas flux. The corresponding film thickness distributions in the tube are shown above.

(B) A region where $\tau_i \gg \tau_w$ and the interface is agitated and wavy over the entire tube. In this case, more liquid enters the tube at the top than can exit at the bottom and a thicker layer of liquid film is built up within the tube. However, due to the associated increased interfacial shear, excess liquid is carried upward by the gas to maintain an equilibrium film thickness. The restriction to countercurrent liquid flow occurs at the tube's bottom end. This region is labelled "rough film" in figure 2.

(C) A transition region where a smooth film exists on the upper portion of the tube and a rough film on the lower portion, with a discontinuity in film thickness appearing somewhere in the middle. The discontinuity may be unstable and oscillate to and fro within the tube. In this region C, the countercurrent flow is limited intermittently at the top and bottom ends and not within the tube.

Typical qualitative variations of liquid flux, liquid fraction, and pressure gradient as functions of the gas flux associated with these regions are also shown in figure 2. The liquid flux j_L^* decreases monotonically with increasing gas flux irrespective of the region. The liquid fraction (averaged over a finite tube length larger than a typical length over which the discontinuity might exist) decreases with increasing gas flux in regions A and B and increases with gas flux in region C. The non-dimensional pressure gradient remains low in region A, increases in region C and attains a value equal to the liquid fraction in region B. For even higher gas fluxes in region D, the liquid film is expelled out of the tube by the gas and the tube becomes dry.

Before discussing the quantitative variation of these characteristics in the three regions, it is helpful to identify other flow situations in fluid mechanics which are analogous to countercurrent flow in circular tubes.

SOME ANALOGIES

When an annular liquid film is present within the tube, the countercurrent flow characteristics are in many ways analogous to flow properties in compressible gas dynamics and/or in open channel flow. The analogies are illustrated in figure 3 for similar flow situations where restrictions to flow can occur at one or two locations in the flow path.

In compressible flow through two deLaval nozzles (typical of supersonic wind tunnels), the subsonic flow is accelerated by supersonic conditions through the first nozzle. Depending on the back pressure, a normal shock can appear in the supersonic stream, behind which the flow is once again subsonic. By suitable adjustment of the throat areas, at a given flux one can achieve within the duct length between the throats, a fully subsonic condition, a fully supersonic condition, or a supersonic and subsonic region separated by a shock. In the case of a fully subsonic flow, the flow is limited at the exit throat; in a fully supersonic flow, it is limited at the entry throat. In cases where a shock is present, the flow is limited at both throats. However, the flow is never limited by the duct between the throats,

The analogies between open channel flow and compressible gas flow are well established, e.g. Bryson (1972). Briefly, for analogous flow in an open channel, when the flow is controlled by two gates, for a given liquid flow, in the region between the gates, one can establish a subcritical flow, a supercritical, or a super and subcritical flow with a hydraulic jump by controlling the gates. In these cases, the flow is limited primarily at the exit gate, at the entry gate, and at both gates, respectively. Here again, the flow is not limited in the region between the gates.

Analogously, in countercurrent flow through a vertical tube, flow limitation can occur at the tube top end, at the bottom end, or at both ends, and does not occur within the tube. By suitably altering the tube end geometries, at given gas and liquid fluxes, one can establish a fully smooth film, a fully rough film or a smooth film followed by a rough film with a discontinuity.

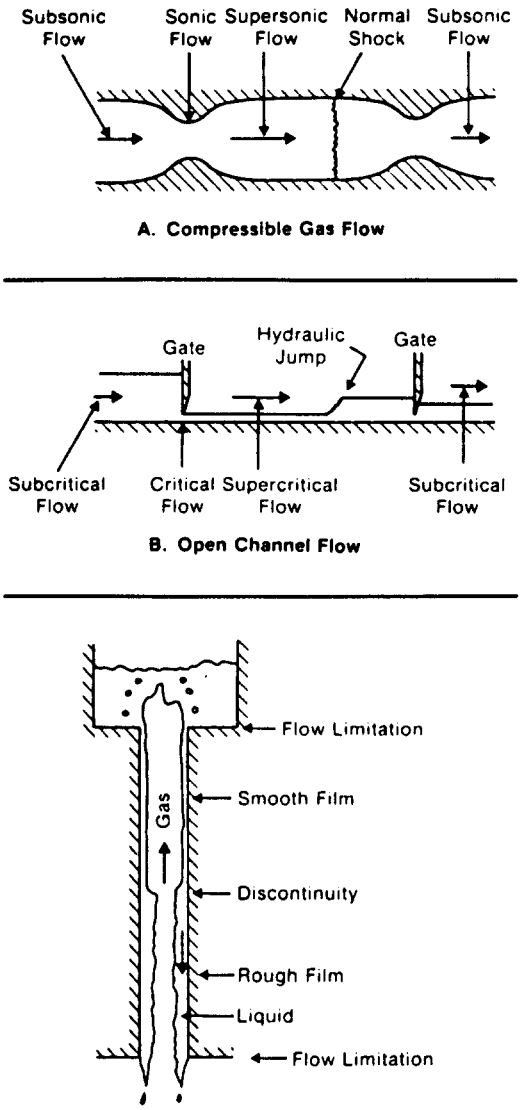

Figure 3. Analogous flow conditions in (a) compressible gas flow, (b) open channel flow and (c) countercurrent annual flow.

For small disturbances, the forces tending to restore the flow back to the original equilibrium arise from bulk compression in gas dynamics, from gravity in open channel flow, and from interfacial shear stresses in countercurrent flow. The nature of the restoring force is conservative in the former two cases, but it is dissipative in countercurrent flow. The analogies and dissimilarities in the three different flow situations are summarized in table 1. Despite many common features, the dissipative nature of the restoring force in countercurrent flow precludes a complete analogy. However, these analogies offer considerable insight into the nature of countercurrent flow in simple straight tubes and the influence of the limiting processes occurring at the tube ends on the observed flow patterns within the tube. The phenomena occurring at the tube ends are, of course, considerably more complicated due to the non-uniformity of the phase distribution and the inherent unsteadiness, and except for identification of the occurrence of the limiting process at the tube's top or bottom end, analyses of the limiting phenomena are beyond the scope of the present work.

Table 1. Analogies and dissimilarities between compressible gas flow, open channel flow and countercurrent flow.

Property	Compressible Gas Flow	Open Channel Flow	Countercurrent Flow
Flow Features	Sonic Flow	Critical Flow	"Ideal" Flooding (i.e., flow properties on the envelope, see Section on Flow Envelopes)
	Supersonic Flow	Supercritical Flow	Smooth Film ($\tau_w >> \tau_i$)
	Subsonic Flow	Subcritical Flow	Rough Film ($\tau_w << \tau_i$)
	Normal Shock	Hydraulic Jump	Discontinuity in Film Thickness
	Choking at Minimum Area	Critical Flow at Channel Entry and/or Exit	Limiting Flow at Tube Entry and/or Exit
Restoring Force	Bulk Compression	Gravity	Interfacial Shear Stress
Nature of Restoring Force	Conservative	Conservative	Dissipative

FURTHER DISCUSSIONS OF FLOODING REGIMES

Smooth film

In *region A*, since the interface is smooth, the limiting mechanism governing the liquid counterflux occurs at the tube's top end geometry and not at the bottom end or within the tube. However, the wall shear stress governs the flow of liquid in a nearly free falling film over the tube length. Viscous effects in the film can be characterized by an effective liquid Reynolds number as

$$\mathrm{Re}_\Gamma = j_L \frac{\rho_L D}{\mu_L} = j_L^* N_L \qquad [11]$$

where μ_L is the dynamic viscosity of the liquid and N_L, is a form of a "Grashof Number" defined as

$$N_L = \frac{\sqrt{(\rho_L(\rho_L - \rho_G)gD)D}}{\mu_L} \qquad [12]$$

Wallis (1969) suggests that for $\mathrm{Re}_\Gamma < 1000$, the flow remains laminar. For laminar flow, the film thickness is related to the liquid flow as

$$\frac{\delta}{D} = \left(\frac{3j_L^*}{4N_L}\right)^{1/3}. \qquad [13]$$

For turbulent flow, based on the correlation for the wall friction proposed by Belkin (1959), Wallis (1969) presents the relation between liquid film thickness and flow rate as

$$\frac{\delta}{D} = 0.063 j_L^{*2/3}. \qquad [14]$$

Given j_L^*, [13] and [14] may be used to estimate the liquid fraction within the tube.

The interfacial shear stress contributes negligibly to support the liquid film and thus the pressure gradient for the gas flow in this region remains rather low and near a value expected for pipes with negligible surface roughness.

Rough film

In *region B*, the liquid film is significantly agitated by the core gas flow over the entire tube length, indicating the presence of a large interfacial shear stress. Cross plots of pressure gradient vs liquid fraction (Bharathan 1978a) indicate that

$$-\left(\frac{dp}{dz}\right)^* \approx (1-\alpha). \qquad [15]$$

In this region, since the flow of either phase is turbulent and since the interface is rough and wavy, momentum transfer between phases is best characterized by an empirical interfacial friction factor as defined earlier. Postulating that the interfacial surface roughness may be governed by surface tension forces, similar to the concept of "equivalent sand roughness", the friction factor f_i may be related to the film thickness δ, surface tension σ, and the pipe diameter D, irrespective of the gas and liquid fluxes, as

$$f_i = 0.005 + \pi_1(\delta, D, \sigma). \qquad [16]$$

The constant 0.005 reflects the fact that the friction factor reaches a finite value corresponding to that for a smooth-walled pipe when the liquid film disappears. π_1 is an arbitrary function yet to be defined.

Equivalently,

$$f_i = 0.005 + \pi_2(\delta^*, D^*) \qquad [17]$$

where δ^* and D^* are non-dimensionalized as

$$\delta^* = \frac{\delta}{\sqrt{\left(\frac{\sigma}{(\rho_L - \rho_G)g}\right)}} \qquad [18]$$

and

$$D^* = \frac{D}{\sqrt{\left(\frac{\sigma}{(\rho_L - \rho_G)g}\right)}} \qquad [19]$$

and π_2 is an altered form of π_1.

The implications of the definition in [17] are:

(1) The valid range of any chosen form of π_1 or π_2 should be restricted to annular flow, i.e. $0 < (\delta^*/D^*) < 0.05$.

(2) For small tubes when D^* is near unity, the liquid film is likely to bridge across the tube and annular flow is not possible. Thus, D^* must be restricted to $D^* > 2$.

(3) When $D^* \gg 1$, the influence of D^* on friction factor should disappear, i.e. the form of π_1 or π_2 should reflect the fact that the behavior of thin films for large pipes should be independent of the pipe diameter. This conclusion is consistent with the observation that for large tubes, the onset of the liquid film penetration during flooding is governed by a constant Kutateladaze number (Pushkina & Sorokin 1969; Wallis 1974) as

$$\mathrm{Ku}_G = j_G^* \sqrt{(D^*)} = 3.2. \qquad [20]$$

For rough films, the liquid flow is limited by the tube's bottom end geometry and not

within the tube or its top end, i.e. more liquid can flow into the tube than can possibly get out at the bottom and thus the amount of the liquid contained within the tube is governed by the interfacial shear stress.

Discontinuity

In *region C*, where a discontinuity in film thickness appears within the tube, the liquid counterflow is limited by both tube ends. The flow in region C may be unsteady, with the location of the discontinuity oscillating within the tube, indicating that the limiting process may alternate between the top and bottom tube ends. The amplitude and frequencies of flow oscillations, of course, will depend upon the characteristics of the fluid supply and supply-line impedance (Bharathan *et al.* 1978b).

Flooding envelope

Even though the mechanism limiting countercurrent flow does not ordinarily occur within the tube, when end effects can be ignored, an "upper limit" to countercurrent flow in the tube can be obtained as follows.

By combining [2] and [7], the gas and liquid flow rates can be related as

$$\frac{2f_i j_G^{*2}}{\alpha^{5/2}} + \frac{2f_w j_L^{*2}}{(1-\alpha)^2} = (1-\alpha). \qquad [21]$$

Provided the friction factors f_i and f_w are known, the limiting values j_L^* and j_G^* can be obtained as an envelope of curves generated with, for example, $(1-\alpha)$ as a parameter.

For the flow conditions on the envelope, the interfacial and wall shear stresses assume equal importance yielding a film which is devoid of an abrupt discontinuity in the film thickness within the tube. This condition is analogous to conditions in the field of gas dynamics to achieve shock-free sonic flow in a uniform duct. Transonic conditions in gas dynamics and ideal flooding conditions corresponding to a point on the envelope of [21] in countercurrent two-phase flow are difficult to achieve in practice unless exceptional care is devoted to the design of entry, exit, and tube geometries, and selection of flow conditions.

EMPIRICAL FRICTION FACTORS

Pressure gradients were measured as a function of j_G^* for a wide range of tube diameters ($2.3 < D^* < 56$) under flooding conditions, Bharathan *et al.* (1979). Data for rough films lend themselves to convenient evaluation of friction factors. Since the pressure gradients associated with this region are generally larger, more accurate measurements are possible even in shorter tubes. Further, since [15] holds good, independent measurement of liquid film thickness is also not necessary. Using [4], interfacial friction factors were deduced as a function of film thickness for each tube.

A relatively simple functional form for π_2 was chosen as

$$\pi_2(\delta^*, D^*) = A\delta^{*B}. \qquad [22]$$

Here A and B are functions of D^* and, based on the experimental data, are best approximated by

$$\log_{10} A = -0.56 + \frac{9.07}{D^*} \qquad [23]$$

and

$$B = 1.63 + \frac{4.74}{D^*}. \qquad [24]$$

For large values of D^*, the parameters A and B approach finite limits as expected. With these values for A and B, the variations of f_i with film thickness δ^*, for various D^* values, are shown in figure 4. At a given δ^*, the friction factor for the smaller tube is larger, since the relative "surface roughness" is larger. When cross-plotted as a function of the liquid fraction $(1-\alpha)$, for all tube sizes, f_i varies over two orders of magnitude for $0 < (1\alpha) < 0.2$. For tube diameters in the range 6 to 25 mm ($2.3 < D^* < 9.4$), these variations merge together sufficiently close to mask any tube diameter dependence. In the case of larger tubes, however, a clearcut dependence on diameter is observed.

The wall friction factor, for tube diameters in the range 1.3 to 15 cm, for smooth walled tubes, can be conveniently assumed, as a first approximation, to be

$$f_w = 0.005. \qquad [25]$$

For smaller diameter tubes, at low Reynolds numbers, f_w is somewhat higher. In these cases, appropriate values of f_w may be used in [21].

Using [22] and [25], complete sets of countercurrent flow characteristics for various tube sizes can be generated. The following sections illustrate important features of the theory and comparisons with experiments.

FLOW ENVELOPES

A typical plot of j_G^* vs j_L^* for various values of $(1-\alpha)$ (from 0.002 to 0.2) for air and water flows at an atmospheric pressure and room temperature (15°C) generated using [21] for a 5.1 cm tube is shown in figure 5. Curves of constant $(1-\alpha)$ would be ellipses if the coordinates were j_G^* and j_L^*. There exists an envelope for this set of curves, a point on which yields the possible maximum j_L^* for a given j_G^* and *vice versa*. The envelope also bounds the

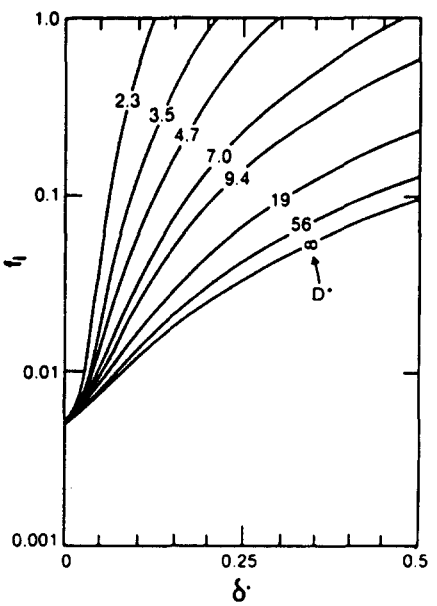

Figure 4. Variation of interfacial friction factor with film thickness δ^* for various tube diameters.

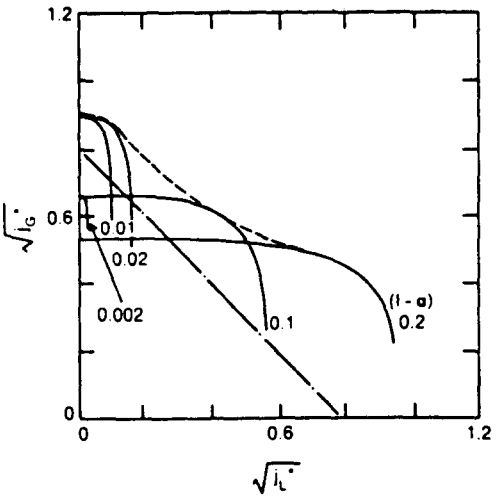

Figure 5. Countercurrent flow envelope generated with curves of constant liquid fraction, $(1-\alpha)$, for a 5.1 cm tube ($D^* = 19$); ————, envelope; ———·———, [9] with $m = 1$ and $C = 0.8$.

possible combinations of flow rates at which any liquid film can be present within the tube. Within the region enclosed by the envelope, at given j_G^* and j_L^* values, two curves, each for a distinct $(1-\alpha)$, intersect yielding two solutions for $(1-\alpha)$.

To achieve maximum possible air and water counterflows on the envelope, under "ideal" flooding conditions, the flow limiting process must occur within the tube and "end effects" must be negligible. However, in practical cases, end effects persist and the measured limiting flows fall within the region enclosed by the envelope, along a line such as the Wallis correlation, [9], with C values in the range 0.7 to 1.0, with smoother, well-rounded end geometries yielding higher C values. Such a line with $C = 0.8$ is shown in figure 5. At any point on this line, there are two possible solutions for $(1-\alpha)$. For the lower $(1-\alpha)$ value, the wall shear stress τ_w is much greater than the interfacial shear stress τ_i; also the pressure gradient $(dp/dz)^*$ is low, close to that for a single-phase air flow. This solution corresponds to a smooth film flow with the flow of either phase being unimpeded by the other. For the solution corresponding to a higher $(1-\alpha)$ the interfacial shear is much greater than the wall shear, with $(dp/dz)^*$ almost equal to $(1-\alpha)$. This second solution corresponds to a rough film where the impedence to flow of either phase arises primarily from the interfacial shear stress. Depending on whether the flow limitation occurs at the top or the bottom, the former or the latter solution will occur within the tube. When the flow is limited at both ends simultaneously, both solutions will occur in different sections of the tube.

The nature of these two solutions is better illustrated in the plot of $(dp/dz)^*$ vs $(1-\alpha)$ in figure 6. For a given flow rate of either phase, [2] and [7] may be represented graphically by curves of constant j_G^* or j_L^*. For a 5.1 cm tube ($D^* = 19$), these curves have been drawn for the particular values of f_i and f_w given by [22] and [25]. The intersections of two such curves, denoted by A and B, yield two solutions for $(1-\alpha)$ and $(dp/dz)^*$, point A corresponding to a low $(1-\alpha)$ and point B to a high $(1-\alpha)$. For j_G^* and j_L^* combinations on the envelope, these two intersections merge into one, yielding only one solution; with further increases in either flow rate, no solution is possible. Curves of constant j_L^* using [7] for downward liquid flow intersect the abscissa at a value of $(1-\alpha)$ corresponding to free-falling film flow. Curves of constant j_G^* from [2] intersect the ordinate at a value of $(dp/dz)^*$ corresponding to a single-phase gas flow.

If the gas and liquid fluxes are limited by the Wallis correlation with, for example, $C = 0.8$, then the operating regions in this figure are confined to the two disconnected cross-hatched regions A and B, corresponding to a smooth film and a rough film,

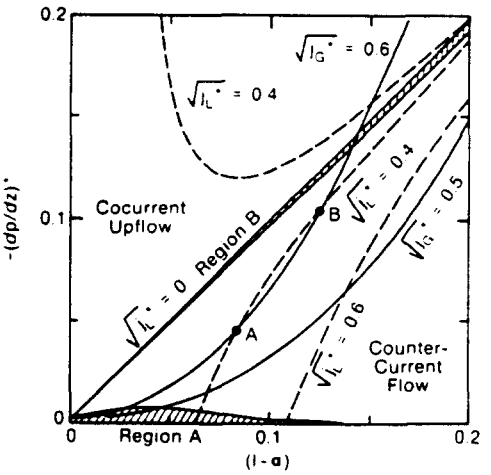

Figure 6. Pressure-gradient vs liquid fraction, simultaneous solution of [2] and [7] for constant values of j_G^* and j_L^*; regions of possible operation in countercurrent flow are shown shaded for flow rates limited by [9] with $C = 0.8$; ————, [7]; ————, [2].

respectively. In the region A, $(1-\alpha)$ is not very different from the value for a free falling film and $(dp/dz)^*$ is close to the value for single-phase gas flow. In the region B, $(1-\alpha)$ is approximately equal to $-(dp/dz)^*$ and close to the value obtained with $j_L^* = 0$. For larger C values, the regions A and B expand and these approximations deteriorate.

Since the regions A and B are not connected, smooth transition from solution *A* to solution *B* is not possible. If these two solutions are to occur simultaneously within the tube, some form of a discontinuity (similar to a hydraulic jump or a normal shock in supersonic flow) in the liquid film thickness and the pressure gradient must be present.

The region below the diagonal line $-(dp/dz)^* = (1-\alpha)$ in figure 6 represents countercurrent flow, while the region above represents cocurrent up flow. For cocurrent flow, for all possible j_G^* and j_L^* values, there occurs one and only one intersection between [2] and [7] indicating a unique solution for both $(1-\alpha)$ and $(dp/dz)^*$ as opposed to the possibility of either one, two, or no solutions in countercurrent flow.

LIQUID FRACTION AND PRESSURE GRADIENT

Both the liquid fraction and pressure gradient within the tube are double-valued functions of j_G^* and j_L^*, whenever these fluxes lie within the region enclosed by the flooding envelope, and are single-valued functions when these fluxes lie on the envelope. For various j_G^* and j_L^* combinations, the $(1-\alpha)$ and $(dp/dz)^*$ variations with j_G^* obtained using [21] for a 5.1 cm tube ($D^* = 19$) can be plotted as in figure 7. For each variable, three different variations, one for $j_L^* = 0$, one for $j_L^* = j_{L\max}^*$ (i.e. along the envelope), and one for flow rate combinations following [9] with $C = 0.8$ are included. For j_G^* and j_L^* values within the flow envelope, the low $(1-\alpha)$ or the smooth-film solutions are denoted by the "A" branch in these figures and the high $(1-\alpha)$ or the rough-film solutions by the "B" branch. For j_G^* and j_L^* combinations on the envelope, these two branches coincide. At a given j_G^*, $(1-\alpha)$ attains a maximum value on the "B" branch when $j_L^* = 0$, and a minimum on the "A" branch when j_L^* is nearly zero. For finite j_L^*, values of $(1-\alpha)$ for the "B" branch are lower and for the "A" branch are higher. The "B" branch for [9] with $C = 0.8$ falls close to that for $j_L^* = 0$ and is indistinguishable in this figure. For the "A" branch, except for the very low $(1-\alpha)$ values, $(1-\alpha)$ varies as the (2/3) power of j_L^* for turbulent film flow indicating that the film can be considered as freely falling. The pressure gradient shown on the right for the "A" branch is low; for the "B" branch, it is nearly equal to $(1-\alpha)$. For the envelope, the two branches coincide.

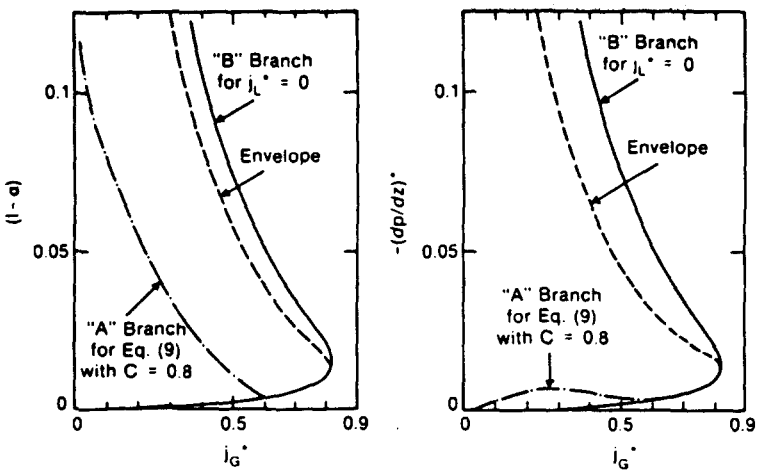

Figure 7. Liquid-fraction and pressure-gradient variations with gas flux for various liquid fluxes for a 5.1 cm tube ($D^* = 19$). ———— Variation for $j_L^* = 0$; — — — —, variation along the envelope; ·—·—·—, variation for Wallis correlation with $C = 0.8$.

EFFECT OF END GEOMETRY ON COUNTERCURRENT FLOW LIMITS

For the 2.5 cm dia. tube ($D^* = 9.4$), limiting fluxes for four different end geometries are shown in figure 8.† The entry radius ratios (R/D) for the four sets were -0.125, 0, 0.75 and 1.5. The negative radius of curvature at the entry implies inwardly curved entries restricting the tube's cross sectional area. For each entry geometry the data cluster around the Wallis correlation with differing C values, with larger entry radius yielding larger values for C. For the case (R/D) = 1.5, a low upper plenum water level allowed increased counterfluxes due to somewhat lesser interaction between the two phases at the liquid entry. For comparison, the limiting envelope generated using [21] is also shown in this figure. The experimental data invariably fall within the envelope. However, these data suggest that for a "correctly" designed entry shape, at the design flow conditions, it may be possible to achieve "ideal" flooding conditions corresponding to a point on the envelope (though it is not clear that a particular end geometry will result in ideal flooding conditions for all possible ranges of gas and liquid fluxes).

For larger tubes, increased radii of curvature at the tube ends resulted in smaller increases in values for C (Bharathan 1979).

LIMITING ENVELOPE FOR LARGE TUBES

For sufficiently large diameter tubes ($D^* > 160$), the interfacial friction factor variation with δ^* can be approximated from [23] and [24] as

$$f_i = 0.005(1 + 55\delta^{*1.63}). \qquad [26]$$

In the case of thin films ($\delta/D < 0.001$), the countercurrent flow in the tube is similar to downward liquid film flow on a plane wall with gas flowing upward adjacent to it. The effect of the tube's radius of curvature or the tube diameter on the limiting physical mechanism should vanish. Such independence can be reflected by introducing proper choices for non-dimensional liquid and gas fluxes. Introducing a liquid flux per unit perimeter Γ_L as

$$\Gamma_L = \frac{Q_L}{\pi D} = \frac{j_L D}{4} \qquad [27]$$

†For complete set of data, see Bharathan *et al.* (1979).

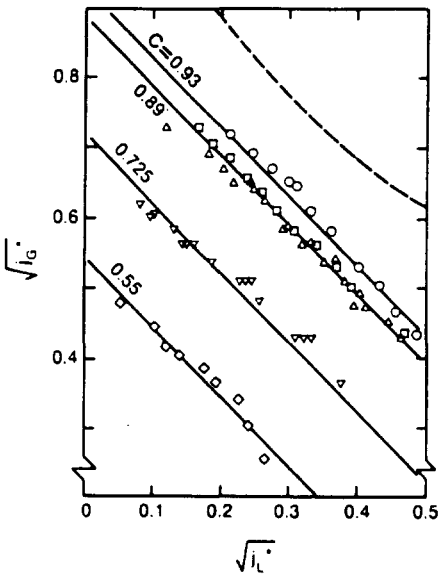

Figure 8. Measured limiting gas and liquid fluxes for a 2.5 cm tube ($D^* = 9.4$) for various end geometries; ◇, $R/D = -0.125$; ▽, $R/D = 0$; △, $R/D = 0.75$; □, $R/D = 1.5$; ○, $R/D = 1.5$, with low upper head water level, ————, envelope.

and defining a dimensionless liquid flow rate as

$$\Gamma_L^* = \frac{\rho_L^{1/2}(\rho_L - \rho_G)^{1/4} g^{1/4} \Gamma_L}{\sigma^{3/4}} = \frac{j_L^* D^{*3/2}}{4} \qquad [28]$$

and approximating,

$$(1-\alpha) \sim 4\frac{\delta^*}{D^*} \quad \text{and} \quad \alpha^{5/2} \sim 1,$$

the force balance, [21], can be written as

$$\frac{1}{2}\left[\frac{f_w}{\delta^{*3}}\right]\Gamma_L^{*2} + \left[\frac{1}{2}\frac{f_i}{\delta^*}\right] \mathrm{Ku}_G^2 = 1. \qquad [29]$$

Since the terms in the square brackets are now functions of δ^* alone and not of the tube diameter D^*, upon elimination of δ^* to find the envelope, the choices of Γ_L^* and Ku_G to represent the liquid and gas fluxes, respectively, yield a universal envelope which is independent of the tube diameter as illustrated in figure 9. The effect of tube diameter on the envelope plotted as $\sqrt{(\mathrm{Ku}_G)}$ vs $\sqrt{(\Gamma_L^*)}$ is shown in this figure. As expected, with increased D^*, the envelope expands, reaching a universal envelope for large D^* in this choice of co-ordinates.

LIMITING OR CRITICAL GAS FLUX

Simultaneous presence of both phases in countercurrent flow within the tube is possible only over a limited range of gas flux. The limiting or critical gas flux is defined as the maximum value of gas flux at which any liquid film can be present within the tube. In countercurrent flow, since the gas flux decreases with increasing liquid flux, the critical gas

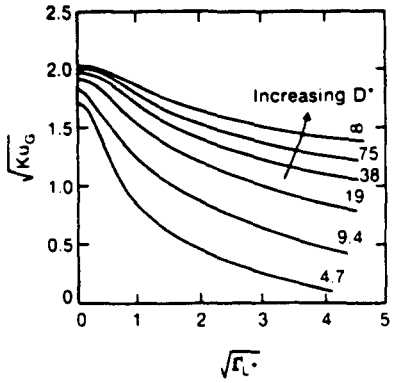

Figure 9. Effect of tube diameter on countercurrent flow envelope. Envelope attains an asymptotic limit for larger tube diameters.

flux occurs when the liquid flux is zero. Thus, it is possible to evaluate the critical gas flux as a function of tube diameter, by letting $j_L^* = 0$ in [21], as

$$\frac{2f_i j_G^{*2}}{\alpha^{5/2}} = \frac{2f_i \mathrm{Ku}_G^2}{\alpha^{5/2} D^*} = (1 - \alpha) \qquad [30]$$

and solving for the maximum of Ku_G.

For sufficiently large tubes ($D^* > 160$), the dependence of f_i on D^* becomes negligible and thus the critical gas flux is independent of the tube diameter. When $D^* > 160$, [30] simplifies to

$$(1 + 55\delta^{*1.63}) \frac{\mathrm{Ku}_G^2}{\delta^*} = 400. \qquad [31]$$

Differentiating this with respect to δ^*, the maximum possible gas flux and the corresponding liquid film thickness are obtained, for large tubes, as

$$\mathrm{Ku}_{G\mathrm{crit}} = 4.189 \qquad [32]$$

and

$$\delta^*_{\mathrm{crit}} = 0.1136. \qquad [33]$$

The maximum value of Ku_G at which any liquid film can be present within the tube as obtained from [30] is plotted as function of D^* in figure 10. For comparison, two other limiting (or "critical") gas fluxes proposed by Wallis (1969) and by Pushkina & Sorokin (1969) are also shown in this figure. Wallis suggested that the liquid film would flow upwards for $j_G^* > 1$, and downward for $j_G^* < 0.5$, and that the critical gas flux would correspond to a line $j_G^* =$ constant in the range $0.5 < j_G^* < 1$. His conclusions were based on data from tubes with diameters in the range 13–18 mm. The investigations of Pushkina & Sorokin indicated that the minimum gas velocity for initial penetration of a liquid film occurred at a constant $\mathrm{Ku}_G = 3.2$ for the tube diameters in the range 6–309 mm. Later experimental investigations by Wallis & Makkenchery (1974) and both experimental and analytical investigations of Wallis & Kuo (1974) indicate that the critical gas flux for liquid film penetration was indeed a function of tube diameter and corresponded to $j_G^* = 0.7$ for $D^* < 15$. For $15 < D^* < 55$, this gas flux gradually tended to an asymptotic limit of

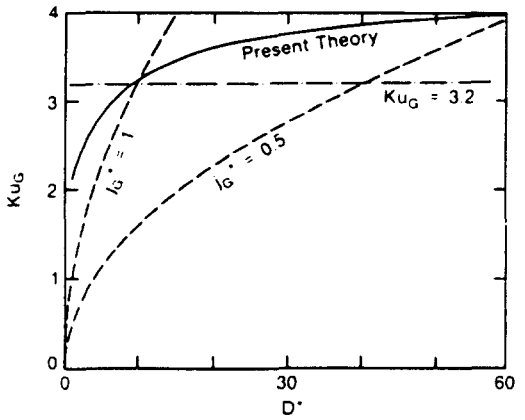

Figure 10. Limiting or critical gas flux as a function of tube diameter D^*; ————, present theory; — — — —, Wallis; ·—·—·—, Pushkina and Sorokin.

$Ku_G = 3.2$. The present limit lies above the previous theories in their range of applicability. It should, however, be noted that there is a subtle but significant difference in the definition of maximum gas flux as referred to in the present and the two earlier predictions. Earlier predictions concern the initial penetration of a liquid film from a pool above and thus are governed by the surface rewetting. The present prediction concerns the maximum gas velocity at which any liquid film (irrespective of how it is introduced in the tube) can be present within the tube and thus is governed by dryout. Thus, on account of the hysteresis associated with dryout and rewetting, the present predictions are greater than the critical gas flux measurements of Pushkina *et al.* (1969), and Wallis (1974).

PRESSURE GRADIENTS

For a tube with a diameter of 1.9 cm ($D^* = 7$), the typical variation of measured pressure gradient is compared to predictions based on empirical wall and interfacial friction factors in figure 11. Since the tube end conditions and the corresponding liquid flux have little influence on the pressure gradient in the rough-film region, only the prediction corresponding to $j_L^* = 0$ is shown. This comparison is somewhat indirect since the two-phase flow predictions are based on the interfacial friction factors which are in turn derived from the measured pressure gradient data. However, the friction factors used here are obtained from the empirical correlations given in [22]–[24] which are based on the data from a wide range of tube diameters. Further, for each tube size, the pressure gradient data have been obtained from at least two different sets of end conditions and a maximum of twelve different sets. Thus, these sets of data establish that irrespective of the flow limitations due to end conditions, for the rough film, the pressure gradient within the tube can be related to the gas and liquid fluxes through the empirical friction factors. The comparisons shown in figure 11 extend over a wide range of gas flux which includes the two-phase flow region up to dryout and the single-phase region past dryout. A clear indication of the typical variation of $(dp/dz)^*$ with j_G^* over the two regions, the associated scatter in the measurements, and the deviation between the predictions and the data can be obtained from this figure.

For all tubes, the measured pressure gradients reported by Bharathan (1979) follow the rough-film predictions closely and decrease with increasing j_G^* until dryout. Near dryout, the data tend to deviate from the rough-film predictions and gradually merge with the dry-tube single-phase predictions.

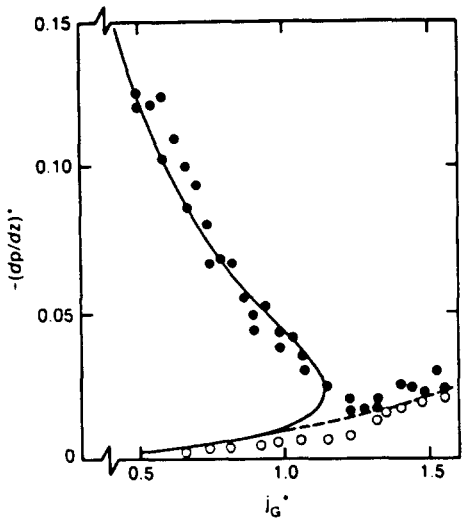

Figure 11. Pressure gradient vs gas flux, for 1.9 cm tube ($D^* = 7.0$); ●, two-phase data; ○, single-phase data; ————, two-phase prediction; ————, single-phase prediction.

CONCLUDING REMARKS

When an annular liquid film is present within a tube, the countercurrent flow characteristics are in many ways analogous to flow features in compressible gas flow or in open-channel flow. For air–water countercurrent flow at atmospheric pressures and temperatures, the empirical interfacial friction factor can be approximated to be a function of only the mean liquid film thickness, and the tube diameter, irrespective of the gas and liquid fluxes. At a given film thickness, the interfacial friction factor decreases with increasing tube diameter, reaching an asymptotic minimum value for large tubes. Based on these friction factors, a simple theory to describe countercurrent flow is developed. The theory is shown to yield solutions corresponding to both smooth-film and rough-film flows. Based on the theory, predicted variations of pressure gradient and liquid fraction with gas flux compare well with experimental measurements. The theory also yields maximum possible air and water fluxes under "ideal" flooding conditions when end effects are minimized. End geometries are shown to affect the limiting air and water fluxes. The influence of end geometries decreases with increasing tube diameters. For large tubes, the choice of correlating parameters for counterfluxes is derived to be the gas Kutateladze number and a non-dimensional liquid flow per unit perimeter. For small tubes the trend of the variation of the critical gas flux deduced from the present theory lies between the predictions based on a constant j_G^* and on a constant Ku_G. For large tubes the maximum possible gas flux for countercurrent flow reaches an asymptotic value of $Ku_G = 4.2$.

Acknowledgements—The reported research was carried out during 1978 and 1979 at the Thayer School of Engineering, Dartmouth College, Hanover, New Hampshire, under research grant 443-2 from the Electric Power Research Institute, Palo Alto, California.

REFERENCES

BELKIN, H. H., MACLEOD, A. A., MONRAD, C. C. & ROTHFOS, R. R., 1959 Turbulent liquid flow down vertical walls. *AIChE J.* 5, 245–248.

BHARATHAN, D., WALLIS, G. B. & RICHTER, H. J. 1978a Air–water countercurrent annular flow in vertical tubes. Electric Power Research Institute Report EPRI-NP-786, Palo Alto, California.

BHARATHAN, D., WALLIS, G. B. & RICHTER, H. J. 1978b Effects of bottom orificing on single- and multi-tube countercurrent flow characteristics. U.S. Nuclear Regulatory Commission Report NRC-0193-6, Washington D.C.

BHARATHAN, D., WALLIS, G. B. & RICHTER, H. J. 1979 Air–water countercurrent annular flow. Electric Power Research Institute Report EPRI-NP-1165, Palo Alto, California.

BRYSON, A. E. 1972 *Principal, 16 mm Sound Film on Waves in Fluids.* Encyclopedia Brittanica Educational Corporation, Chicago, Illinois.

CETINBUDAKLAR, A. G. & JAMESON, G. J. 1969 The mechanism of flooding in vertical countercurrent two-phase flow. *Chem. Engng Sci.* **24**, 1669–1680.

HEWITT, G. F. & HALL-TAYLOR, N. S. 1970 *Annular Two-Phase Flow.* Pergamon, Oxford.

HEWITT, G. F. & WALLIS, G. B. 1963 Flooding and associated phenomena in falling film flow in a vertical tube. U.K. Atomic Energy Research Establishment Report AERE-R4022, Berkshire, England.

IMURA, H., KUSUDA, H. & FUNATSU, H. 1977 Flooding velocity in a countercurrent annular two-phase flow. *Chem. Engng Sci.* **32**, 79–87.

LAHEY, R. T., JR. 1977 *The Thermal-Hydraulics of a Boiling Water Nuclear Reactor*, p. 83. American Nuclear Society, Monograph Series on Nuclear Science and Technology.

PUSHKINA, O. L. & SOROKIN, Y. L. 1969 Breakdown of liquid film motion in vertical tubes. *Heat Transfer—Sov. Res.* **1**, 55–64.

SHEARER, C. J. & DAVIDSON, J. R. 1965 The investigation of standing wave due to gas blowing upwards over a liquid film; its relation to flooding in wetted-wall columns. *J. Fluid Mech.* **22**, 321–336.

TIEN, C. L. & LIN, C. P. 1979 Survey on vertical two-phase countercurrent flooding. Electric Power Research Institute Report EPRI NP-984, Palo Alto, California.

WALLIS, G. B. & KUO, J. T. 1974 The behavior of gas–liquid interfaces in vertical tubes. *Int. J. Multiphase Flow* **2**, 521–536.

WALLIS, G. B. 1970 Flooding in stratified gas–liquid flow. Dartmouth College Report 27327-9, Hanover, New Hampshire.

WALLIS, G. B. & MAKKENCHERY, S. 1974 The hanging film phenomenon in vertical annular two-phase flow. *J. Fluids Engng* 297–298.

WALLIS, G. B. 1969 *One-Dimensional Two-Phase Flow*, p. 336. McGraw Hill, New York.